arXiv:2511.12110v3 [cs.CV] 10 Mar 2026

MediRound: Multi-Round Entity-Level Reasoning Segmentation in Medical Images

Qinyue Tong
Zhejiang University
Hangzhou, Zhejiang, China
qinyuetong@zju.edu.cn

Ziqian Lu
Zhejiang Sci-Tech University
Hangzhou, Zhejiang, China
ziqianlu@zju.edu.cn

Jun Liu
Zhejiang University
Hangzhou, Zhejiang, China
junliu0930@zju.edu.cn

Rui Zuo
Zhejiang University
Hangzhou, Zhejiang, China
22431088@zju.edu.cn

Zheming Lu
Zhejiang University
Hangzhou, Zhejiang, China
zheminglu@zju.edu.cn

Yueming Jin
National University of Singapore
NUS, Singapore
ymjin@nus.edu.sg

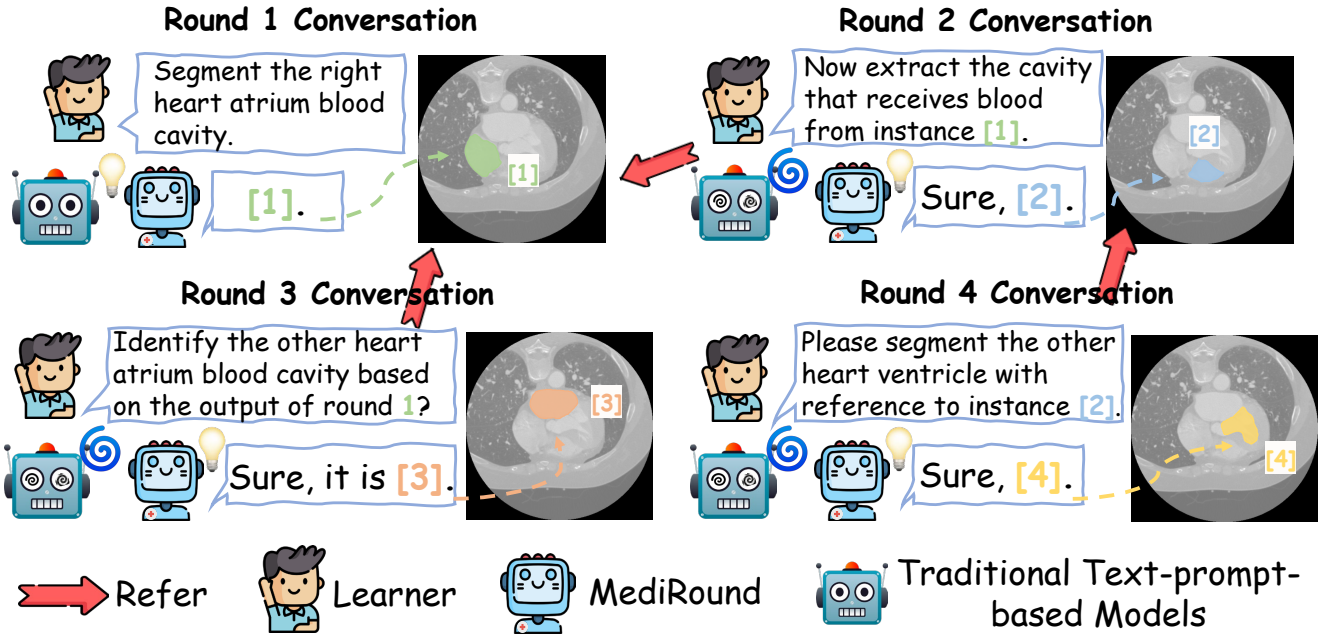

Figure 1. A medical education dialogue illustrating the proposed MediRound. Our model can comprehend user queries that refer to the mask results from previous rounds (*e.g., the Round 2 query refers to the Round 1 mask result*), enabling cross-round entity-level reasoning in multi-round medical conversations. This iterative querying paradigm allows learners to progressively develop their understanding of medical entities. In contrast, conventional text-prompt-based medical segmentation methods struggle with such a complex and context-dependent task.

Abstract

*Despite recent progress in text-prompt-based medical image segmentation, these methods are limited to single-round dialogues and fail to support multi-round reasoning, which is important for medical education scenarios. In this work, we introduce Multi-Round Entity-Level Medical Reasoning Segmentation (**MEMR-Seg**), a new task that requires generating segmentation masks through multi-round queries with entity-level reasoning, helping learners progressively develop their understanding of medical knowledge. To support this task, we construct **MR-MedSeg**, a large-scale dataset of 177K multi-round medical segmentation dialogues, featuring entity-based reasoning across rounds. Furthermore, we propose **MediRound**, an effective baseline model designed for multi-round medical reasoning segmentation. To mitigate the inherent error propagation within the chain-like pipeline of multi-round segmentation, we introduce a lightweight yet effective **Judgment & Correction Mechanism** during model inference. Experimental*

results demonstrate that our method effectively addresses the MEMR-Seg task and outperforms conventional medical referring segmentation methods. The project is available at https://github.com/Edisonhimself/MediRound.

1. Introduction

Medical image segmentation seeks to precisely delineate regions of interest (e.g., organs and lesions) across diverse medical imaging modalities [28, 31, 41]. This capability underpins a broad range of downstream medical applications, including clinical analysis, medical education, and biomedical research [4, 15, 27, 43, 45]. Most existing studies focus predominantly on task-specific segmentation [9, 26, 34], commonly referred to as "specialist models". Despite their remarkable performance, these models generally suffer from limited adaptability and lack the interactive capabilities necessary for practical, real-world usage.

Recent advancements in text-prompt-based medical image segmentation [6, 11, 20, 50] overcome this limitation by allowing users to actively guide the model via simple textual queries, thereby enabling more diverse and user-driven segmentation outcomes. Building upon these developments, several MLLM-based approaches [13, 39, 46] further enhance the interactivity and practicality by enabling reasoning-driven medical segmentation, allowing users to obtain the desired masks through implicit queries.

However, these models primarily focus on single-round medical segmentation and are incapable of supporting multi-round and continuous text-based interactions. Although the one-shot querying paradigm can be efficient in clinical use, it presumes high-quality prompts and substantial user expertise. As a result, it is well suited to medical experts but less conducive to the learning process of **non-expert users**. In **medical education** settings, visual understanding is typically developed **progressively**. As illustrated in Figure 1, learners tend to formulate new segmentation queries based on the mask results obtained from previous rounds. For example, in *Round 2 Conversation*, the user's query is based on the mask generated in *Round 1 Conversation*, and the results of *Round 2 Conversation* in turn serve as a reference for *Round 4 Conversation*. Such iterative questioning helps learners progressively develop a better visual understanding of different medical entities and grasp the relationships among them more effectively. Moreover, these follow-up queries are often relation-driven and logically constrained, reflecting how trainees learn anatomy and pathology through relational concepts rather than precise standalone descriptions, which aligns with how learning occurs in real-world medical education. Unfortunately, due to the lack of multi-round entity-level reasoning capabilities, existing methods often fail to produce the expected responses when dealing with inputs that involve cross-round logical dependencies.

In this work, we define a new medical vision task, termed **MEMR-Seg** (Multi-Round Entity-Level Medical Reasoning Segmentation), which entails generating binary segmentation masks based on multi-round medical image queries, involving entity-level reasoning across dialogue rounds. Notably, the queries are not only multi-round in nature, but each round is also a derivative and extended inquiry based on the entity results from the previous round. To successfully perform this task, the model should possess two essential capabilities: *(1) supporting multi-round dialogue and cross-round entity-level reasoning*; and *(2) generating accurate segmentation results in response to user queries*.

Given that data scarcity represents a major bottleneck in accomplishing MEMR-Seg, we first introduce a Multi-Round Entity-Level Medical Reasoning Segmentation dataset, termed **MR-MedSeg**, which contains a large number of medical conversations centered on entity-level reasoning segmentation with multi-round queries and answers. We collect all metadata from the publicly available SA-Med2D-20M [48]. Subsequently, inspired by SegLLM [42], we construct multi-round question–answer pairs through a combination of manual annotation and GPT-5-based generation. As a result, the MR-MedSeg dataset comprises a large and diverse collection of 177K conversations. Notably, a key distinction between the proposed MR-MedSeg and traditional medical segmentation datasets [2, 10, 35–37, 39] lies in the fact that our dataset not only features multi-round dialogues but also incorporates entity-based reasoning logic across different dialogue rounds. This design enhances the educational utility of MR-MedSeg and facilitates more interactive medical image segmentation.

Furthermore, building upon existing reasoning-based segmentation works [18, 40, 42, 47], we introduce **MediRound**, an effective baseline model designed for multi-round medical reasoning segmentation. MediRound integrates the segmentation feature representations from the reference round and the textual information from previous dialogues with the current query. These are jointly embedded into the input sequence of the inner-MLLM. This design enables the model not only to comprehend the current query but also to access the core information from the reference round while maintaining awareness of the entire conversational history. Moreover, to address the inevitable issue of error accumulation inherent in multi-round segmentation (*as illustrated in Figure 1, if the result of Round 1 contains errors, these errors may propagate to Round 2, and the resulting inaccuracies in Round 2 can further affect Round 4*), we introduce a lightweight yet effective **Judgment & Correction Mechanism** during the model inference stage. Applied after the end-to-end model training phase, this mechanism helps MediRound mitigate er-

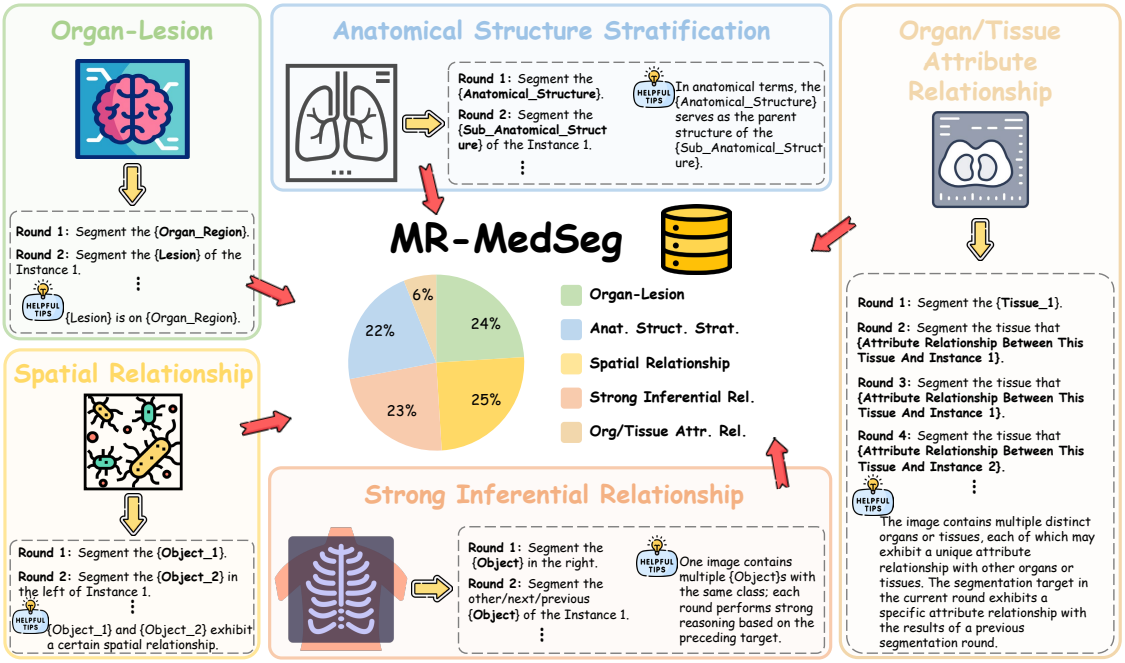

Figure 2. Overview of MR-MedSeg. Our dataset comprises five types of medical reasoning dialogues, each characterized by a specific form of inter-instance relationship, encompassing nearly all multi-round interaction scenarios encountered in real-world medical applications.

ror propagation in practical multi-round inference and effectively enhances the overall accuracy of multi-turn entity-level reasoning. Extensive experimental results demonstrate the superior performance of MediRound in both multi-round and single-round medical segmentation, while confirming the effectiveness of the Judgment & Correction Mechanism. Overall, we summarize our main contributions as follows:

- We introduce the Multi-Round Entity-Level Medical Reasoning Segmentation (**MEMR-Seg**) task, which requires reasoning over multi-round queries that refer to results from earlier rounds in medical images.
- We construct the **MR-MedSeg** dataset, which comprises 177K multi-round medical segmentation dialogues that require multi-round reasoning.
- We propose an effective baseline model, **MediRound**, and introduce a **Judgment & Correction Mechanism** to address the inherent error accumulation during multi-round reasoning segmentation. Extensive experiments demonstrate the superior performance of our model and the utility of the proposed mechanism.

2. Related Works

Medical Image Segmentation. As one of the foundational architectures in medical image segmentation, the U-Net family [7, 14, 34, 51] has inspired numerous extensions and variants. Despite their strong performance on specific tasks and imaging modalities, these fully automated and task-specific models often lack the flexibility and user interactivity necessary for adaptability in practical, real-world medical environments. Text-prompt-based segmentation models address this by allowing clinicians to guide segmentation via language prompts [6, 8, 24, 50], and recent works further support complex implicit queries [13, 39, 46], improving flexibility and interactivity. However, they cannot handle continuous, multi-turn queries or perform cross-round reasoning over medical entities. In this work, we focus on multi-round entity-based medical reasoning segmentation, enabling entity-centered reasoning across dialogue rounds while generating accurate segmentation masks.

Reasoning Segmentation. Reasoning segmentation in natural images is introduced by LISA [18], which interprets implicit textual instructions to generate segmentation masks by combining MLLMs' vision-language understanding [21] with SAM's segmentation capabilities [17]. More recently, several follow-up studies extend reasoning segmentation [16, 29, 32, 49]. Among them, SegLLM [42] represents the initial effort to address multi-round reasoning segmentation in natural images. Compared to natural image domains, multi-round reasoning segmentation in medical imaging may provide greater practical value. This is because such a segmentation paradigm can not only assist clinicians in performing rapid, continuous segmentation during clinical practice, but also help lay users learn medical knowledge more effectively. However, despite recent progress in medical reasoning segmentation [13, 39, 46], this aspect remains unaddressed. In this paper, building upon existing works [19, 25, 42, 48], we develop a method

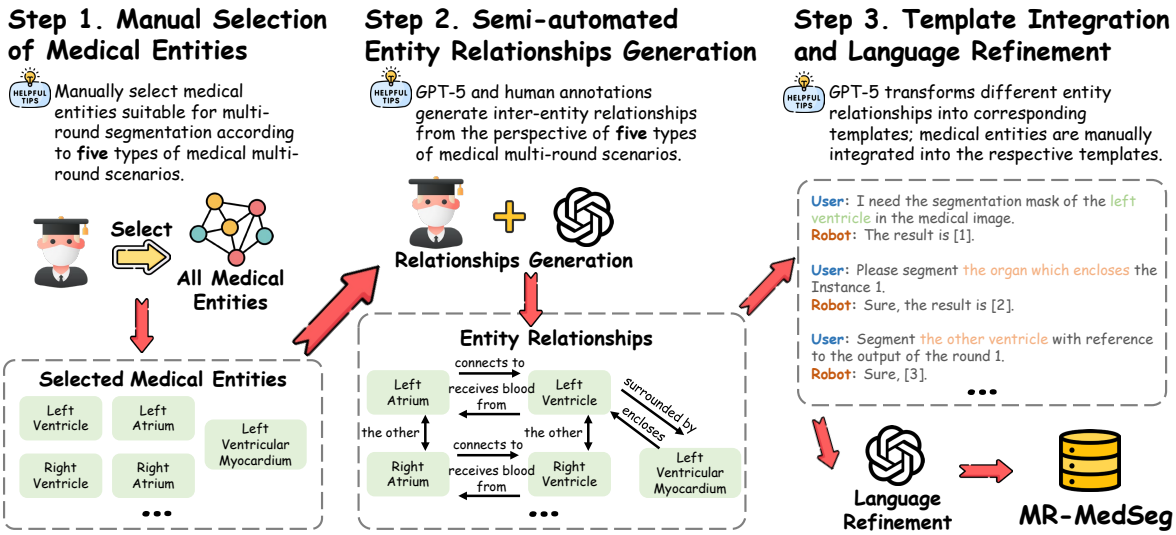

Figure 3. Semi-automatic pipeline for constructing MR-MedSeg dataset. The process includes three stages: entity selection, relationship generation, and template integration. The pipeline is primarily driven by manual annotation and complemented by GPT-5–based generation.

for multi-round reasoning in medical image segmentation.

3. MR-MedSeg

Dataset Overview. The overview of our proposed MR-MedSeg dataset is shown in Figure 2. As illustrated in the figure, we design five representative types of interaction scenarios tailored for multi-round entity-level medical reasoning segmentation, each reflecting realistic use cases in medical education practice. These scenarios each involve distinct forms of inter-instance relationships, including organ–lesion dependency, anatomical hierarchy, organ/tissue attribute association, spatial relationship, and strong inferential relationship. Figure 2 further presents the overall composition and proportions of these scenarios in MR-MedSeg. *Additional detailed descriptions of each scenario and their corresponding inter-instance characteristics are provided in the Appendix.*

Data Construction Pipeline. As illustrated in Figure 3, we design a semi-automatic pipeline for constructing the MR-MedSeg dataset. The details are as follows.

In *Step 1*, we manually select appropriate medical entities according to the five types of multi-round medical interaction scenarios illustrated in Figure 2. Specifically, we traverse the SA-Med2D-20M dataset [48] and identify sub-datasets that meet the criteria of each scenario. From these selected sub-datasets, we further manually select the medical entities that best match the five designed interaction settings. The high-quality images, masks, and labels from SA-Med2D-20M serve as the foundation for MR-MedSeg, greatly reducing the effort required for data pre-processing and annotation. Next, in *Step 2*, we construct diverse inter-entity relationships for the selected medical entities based on the entity relationships defined across five scenarios, employing a hybrid strategy that combines *manual annotation* with *GPT-5–based generation*. Notably, when generating relationships that are independent of image information, such as biological or anatomical attributes shared among medical entities which are generally consistent across images, we omit the reference to the image context. In contrast, when generating relationships that depend on image information, such as the relative spatial positions of anatomical structures that vary between images, we explicitly incorporate the corresponding image context to ensure both accuracy and contextual relevance. Subsequently, in *Step 3*, we employ GPT-5 [1] to transform each entity relationship into 50–80 diverse yet semantically equivalent templates. The corresponding medical entities are then manually integrated into these templates to construct the initial version of the multi-round medical segmentation data. Finally, we perform an additional automatic refinement process using GPT-5 to further enhance the fluency and accuracy of the generated dialogues. Moreover, we engage three inspectors with professional medical expertise to screen and filter the data in MR-MedSeg, thereby maximizing the validity and reliability of the dataset.

Data Statistics. The MR-MedSeg dataset comprises over 177K multi-round medical segmentation dialogues that require cross-round reasoning, along with 118K images and 569K masks. We allocate 174,934 conversations to the training set, 1,270 to the validation set, and 1,273 to the test set. In addition, MR-MedSeg encompasses a comprehensive set of 168 medical entity categories, including various types of organs, lesions, and tissues. The dataset also covers 9 medical imaging modalities, further highlighting its diversity. *More detailed quantitative analyses and data examples of the dataset are provided in the Appendix.*

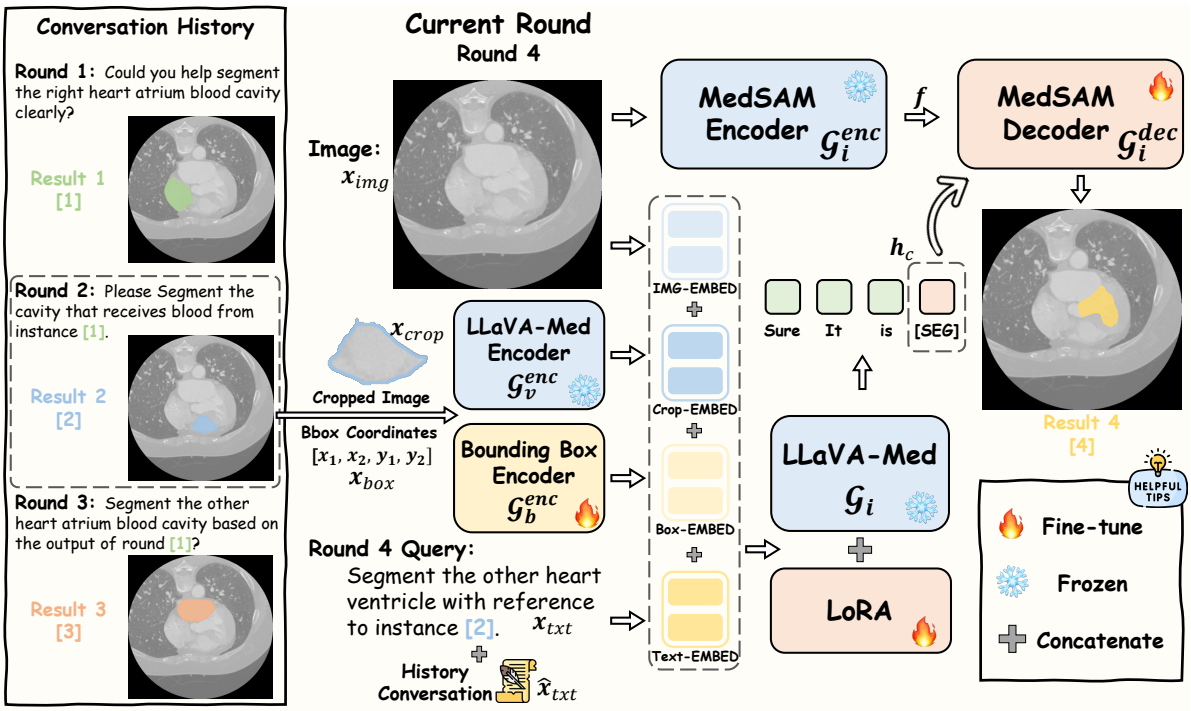

Figure 4. Overview of the MediRound framework. The figure illustrates the model's workflow in processing the fourth-round conversation, referring to the second-round mask. The llava-med encoder $\mathcal{G}_v^{enc}$ consists of the vision encoder and visual projection layer from llava-med.

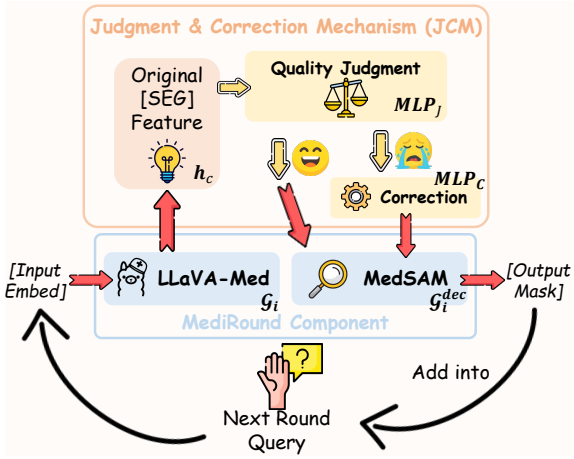

Figure 5. Illustration of how the Judgment & Correction Mechanism assists MediRound in multi-round reasoning. This mechanism evaluates and optimizes the quality of the [SEG] hidden layer features in each round, effectively preventing current-round errors from being propagated to later dialogues. Notably, the mechanism is not involved in the end-to-end training of MediRound and is only introduced during the evaluation process of the model.

4. Baseline Framework

We propose an effective baseline architecture for multi-round medical reasoning segmentation, termed MediRound. MediRound demonstrates the ability to perform multi-round reasoning over segmented medical entities by understanding information from preceding rounds to achieve fine-grained segmentation in the current round. To address the inherent drawback that errors in previous rounds can severely affect the performance of subsequent rounds in multi-round segmentation pipeline, we introduce a novel Judgment & Correction Mechanism (JCM). Details of MediRound and JCM follow.

Model Architecture. Figure 4 illustrates the overall architecture of our proposed MediRound, which is composed of four core components: MedSAM [25] serving as the vision backbone with an image encoder $\mathcal{G}_i^{enc}$ and a mask decoder $\mathcal{G}_i^{dec}$; LLaVA-Med [19] functioning as the multimodal large language foundation model $\mathcal{G}_i$; the LLaVA-Med visual encoder $\mathcal{G}_v^{enc}$ for extracting and projecting image embeddings; and a linear projection acting as the bounding box encoder $\mathcal{G}_b^{enc}$.

Multi-Round Reasoning and Segmentation. Inspired by existing MLLM-based (*e.g., LLaVA* [21]) segmentation methods [16, 47, 49] and the pioneer in general multi-round segmentation method SegLLM [42], we propose the MediRound tailored for multi-round medical reasoning segmentation. Specifically, we first extend the original LLM vocabulary by introducing a special token, [SEG], which denotes a request for segmentation output. As shown in Figure 4, **three rounds of conversations have already been established**. Given the **Round 4** query x_{txt} together with the original input image x_{img} and history conversation $\hat{x}_{txt}$ (including the question–answer pairs from Rounds

Table 1. Comparison of multi-round entity-level medical reasoning segmentation performance between MediRound and prior related methods. *"regular case"* refers to relatively regular reasoning dialogues, whereas *"hard case"* denotes more challenging ones, which involve more complex reasoning and dialogues with a greater number of turns. $\mathcal{T}$ denotes whether the method is an independent model (a single model or with an extension). This table reports the overall scores across all rounds in the MR-MedSeg dataset.

Methods	val			test						$\mathcal{T}$
	overall			regular case			hard case			
	Dice	gIoU	cIoU	Dice	gIoU	cIoU	Dice	gIoU	cIoU	
Human-Thinking + BiomedParse [50]	21.1	17.0	12.1	28.6	22.1	19.0	11.3	10.2	8.4	✗
Human-Thinking + MedPLIB [12]	33.7	25.3	24.5	35.0	24.8	24.7	32.0	25.2	23.4	
Human-Thinking + IMIS-Net [6]	30.5	25.9	32.2	33.7	30.0	42.6	26.4	21.0	25.3	
Human-Thinking + MediSee [39]	43.0	33.5	35.4	45.6	34.5	38.6	45.1	37.1	39.7	
GPT-4o [1] + IMIS-Net [6]	19.3	15.8	19.6	23.8	18.7	20.8	17.4	15.2	21.2	✗
Gemini-2.5-Pro [38] + IMIS-Net [6]	26.9	22.6	28.0	33.6	29.5	35.2	21.9	17.0	19.2	
Qwen3-VL [3] + IMIS-Net [6]	26.6	22.8	26.0	25.1	22.3	26.2	23.4	18.3	20.1	
GPT-4o [1] + MediSee [39]	36.8	28.7	29.4	45.2	34.2	38.0	33.4	26.8	28.9	
Gemini-2.5-Pro [38] + MediSee [39]	33.5	26.1	27.6	37.9	31.4	35.1	38.6	28.6	30.8	
Qwen3-VL [3] + MediSee [39]	42.7	34.0	34.5	45.2	34.1	38.0	37.8	31.4	32.8	
SegLLM-7B [42]	36.3	27.5	36.8	42.1	32.9	42.4	30.4	22.2	31.0	✓
SegLLM-13B [42]	38.9	31.2	39.1	45.3	33.4	44.0	33.0	24.6	33.9	
MediRound + READ [30]	53.9	45.1	54.6	60.3	51.4	57.6	47.2	36.8	49.1	✓
MediRound	55.8	46.5	55.8	61.0	52.1	58.9	48.1	38.2	50.2	
MediRound + JCM	**58.4**	**49.0**	**58.9**	**63.3**	**54.5**	**60.2**	**50.3**	**40.5**	**53.4**	

1, 2, and 3), we first utilize the mask output from the **reference round (Round 2)** to crop the corresponding object x_{crop} from the original image. The cropped region and its bounding box coordinates x_{box} in the original image are used as reference information for the referred medical entity. Subsequently, the LLaVA-Med visual encoder $\mathcal{G}_v^{enc}$ and the bounding box encoder $\mathcal{G}_b^{enc}$ are employed to extract their respective features, which are then concatenated with x_{txt}, $\hat{x}_{txt}$ and x_{img} to form the complete input. This input design enables the model not only to comprehend the current query but also to access key information from the reference round while maintaining awareness of the full conversational history. We then feed the complete input into the MLLM LLaVA-Med $\mathcal{G}_i$, which in turn outputs a text response $\hat{y}_{txt}$. It can be formulated as:

$$\hat{y}_{txt} = \mathcal{G}_i(x_{img}, \mathcal{G}_v^{enc}(x_{crop}), \mathcal{G}_b^{enc}(x_{box}), x_{txt}, \hat{x}_{txt}). \tag{1}$$

The output $\hat{y}_{txt}$ includes the special token [SEG] when the model intends to segment a specific medical entity within x_{img}. We then extract the last-layer embedding of the LLM corresponding to the [SEG] token, denoted as h_c, which encapsulates the rich semantic representation of the medical entity inferred by the MLLM. Finally, the dense visual features f, extracted from the input image x_{img} by the vision backbone $\mathcal{G}_i^{enc}$, are fed into the decoder $\mathcal{G}_i^{dec}$ together with h_c to generate the target segmentation mask $\hat{\mathbf{M}}$. The process can be formulated as:

$$f = \mathcal{G}_i^{enc}(x_{img}), \quad \hat{\mathbf{M}} = \mathcal{G}_i^{dec}(f, h_c). \tag{2}$$

Algorithm 1 Multi-Round Inference of MediRound with Judgment & Correction Mechanism

Require: Image x_{img}; multi-round queries $\{x_{txt}^{(t)}\}_{t=1}^{T}$; $\mathcal{G}_i$: LLaVA-Med; $\mathcal{G}_i^{dec}$: MedSAM decoder; h_c: [SEG] feature; MLP$_J$: Quality Judgment Module; MLP$_C$: Correction Module; β: the threshold used by Quality Judgment Module to judge the quality of [SEG] feature
Ensure: Predicted masks $\{\hat{\mathbf{M}}^{(t)}\}_{t=1}^{T}$

```
M̂^(0) ← ∅
for t = 1 to T do
    x̃_txt^(t) ← IntegrateMaskInfo(x_txt^(t), M̂^(t−1))
    h_c ← G_i(x_img, x̃_txt^(t))
    q ← MLP_J(h_c)
    if q > β then
        M̂^(t) ← G_i^dec(h_c)
    else
        h'_c ← MLP_C(h_c); M̂^(t) ← G_i^dec(h'_c)
    end if
end for
```

Judgment & Correction Mechanism. During the training of MediRound, we adopt teacher forcing [44] and directly use the ground truth masks to obtain the referred information. While this strategy effectively optimizes the model parameters, it introduces a discrepancy between the training and testing scenarios: *during multi-round evaluation, the trained model can only rely on its own outputs from previous rounds as reference information*. As illustrated in Figure 4, the mask information from the referred round provides essential contextual guidance for the current round. This dependency introduces a potential limitation: errors from earlier segmentation rounds may accumulate and propagate, ultimately degrading the accuracy of subsequent predictions during evaluation. This effect may become increasingly pronounced as the number of segmen-

Table 2. Multi-round entity-level medical reasoning segmentation performance of MediRound and prior related methods, reported for each round. The table presents the cIoU scores from rounds #2–#8 across all MR-MedSeg validation samples.

Methods	Conversation Rounds						
	Round #2	Round #3	Round #4	Round #5	Round #6	Round #7	Round #8
Human-Thinking + BiomedParse [50]	13.3	17.9	13.9	15.9	11.5	9.4	7.8
Human-Thinking + MedPLIB [12]	19.7	21.0	21.3	19.7	20.5	25.0	34.4
Human-Thinking + IMIS-Net [6]	34.0	27.1	30.1	33.4	37.5	37.7	32.8
Human-Thinking + MediSee [39]	43.6	37.0	34.4	31.9	29.7	37.0	25.1
GPT-4o [1] + IMIS-Net [6]	25.1	20.4	18.1	17.0	11.6	12.5	18.9
Gemini-2.5-Pro [38] + IMIS-Net [6]	27.2	28.6	29.4	26.2	22.6	20.1	30.5
Qwen3-VL [3] + IMIS-Net [6]	25.6	24.1	20.3	21.8	15.2	14.8	27.6
GPT-4o [1] + MediSee [39]	37.7	33.4	27.3	25.5	14.9	21.5	20.9
Gemini-2.5-Pro [38] + MediSee [39]	30.8	30.4	29.5	26.7	31.5	21.5	33.3
Qwen3-VL [3] + MediSee [39]	37.7	33.9	30.1	25.4	20.2	34.7	29.9
SegLLM-7B [42]	35.2	39.5	27.2	30.1	34.7	37.4	34.1
SegLLM-13B [42]	36.4	42.1	32.5	33.2	35.3	39.6	36.0
MediRound + READ [30]	49.1	58.3	55.0	56.2	62.4	63.3	44.5
MediRound	50.2	60.8	55.9	58.8	63.7	64.7	46.1
MediRound + JCM	**52.6**	**63.6**	**59.7**	**64.6**	**69.5**	**66.3**	**54.8**

tation rounds increases, due to the progressive accumulation and amplification of errors. Therefore, we introduce a lightweight yet effective Judgment & Correction Mechanism that enables the model to transfer higher-quality masks from previous rounds to subsequent ones during evaluation, thereby mitigating the accumulation of segmentation errors. Specifically, as illustrated in Figure 5, during the MediRound evaluation process, we employ a **Quality Judgment Module** to assess the quality of the hidden features associated with the output [SEG] token in the current round. If the feature quality is deemed unsatisfactory, the features are then passed to the **Correction Module** for feature refinement; otherwise, they are directly decoded into masks. In this way, when subsequent rounds refer to the current round result, they receive higher-quality reference mask, which facilitate more coherent cross-round reasoning. To more clearly illustrate how JCM assists MediRound in performing multi-round reasoning, we present the pseudocode of the process in Algorithm 1. Notably, both the Quality Judgment and Correction Modules are implemented as lightweight MLPs. To train them, we freeze all parameters of the end-to-end trained MediRound and leverage the frozen MediRound weights to independently optimize the two modules in a fast and efficient manner. *Further training details of JCM are presented in the Appendix.*

5. Experiments

5.1. Experimental Setting

Network Architecture. For **MediRound**, as described in Sec. 4, we employ LLaVA-Med-v1.5-Mistral-7B [19] as the MLLM, and MedSAM [25] as the vision backbone. The $\mathcal{G}_b^{enc}$ is implemented as a linear projection from 4 dimensions to 4096. For **JCM**, the projections in the Quality Judgment Module and Correction Module are implemented as three-layer MLPs with dimensions [256, 512, 512, 1] and [256, 512, 512, 256], respectively.

Table 3. Vanilla medical referring segmentation results.

Methods	Metrics		
	Dice	gIoU	cIoU
Medical Interaction Seg. (bbox input)			
MedSAM [25]	77.7	67.1	81.0
IMIS-Net [6]	77.0	67.5	87.2
Medical Referring Seg.			
Grounding DINO [22] + SAM-Med2D [5]	18.4	12.5	10.9
Grounding DINO [22] + MedSAM [25]	18.5	11.0	13.5
BiomedParse [50]	24.9	20.1	14.5
MedPLIB [12]	40.6	39.1	45.2
IMIS-Net [6]	41.3	35.5	65.8
MediSee [39]	61.2	**50.4**	**70.8**
MediRound + READ [30]	60.7	48.0	65.2
MediRound	**62.1**	48.3	66.3

Implementation Details. **MediRound** is trained on the MR-MedSeg dataset using four NVIDIA RTX A6000 GPUs (48 GB memory each) for approximately 1.5 days. The batch size per device is set to 15. To enhance training efficiency, we adopt the DeepSpeed [33] engine. Optimization is performed using the AdamW [23] optimizer with a learning rate of 0.0003. Learning rate scheduling is managed by the WarmupDecayLR scheduler, with a warm-up phase spanning 100 iterations. The LoRA rank is uniformly set to 8. For training **JCM**, we keep the same hyperparameter settings, and it can be completed in just half a day. All training is conducted on the MR-MedSeg training set, employing a teacher forcing strategy [44].

5.2. Multi-Round Experimental Results

The results of multi-round medical reasoning segmentation are summarized in Tables 1 and 2. Table 1 reports the overall performance across all rounds, while Table 2 provides detailed scores for each individual round of interaction. Since existing text-prompt-based medical segmen-

tation methods lack the capability for multi-round entity-level reasoning segmentation, we first incorporate human guidance to enable a broader and more equitable comparison. Specifically, humans with medical expertise assist traditional segmentation models through multi-round reasoning, allowing these models to perform the task. As shown in Tables 1 and 2, human assistance can substantially improve the model's ability to perform multi-round segmentation. However, the overall performance remains suboptimal. This is primarily because, even with a certain level of medical knowledge, humans may still make errors when dealing with complex multi-round medical reasoning tasks, and their coordination with the model tends to be relatively rigid. In contrast, the proposed MediRound can effectively comprehend the current query while simultaneously integrating historical information and mask results from referred rounds. By achieving this capability, it demonstrates an average improvement of approximately 15% across various evaluation metrics compared to other methods. Notably, despite its lightweight design, the proposed JCM remarkably improves the model's overall performance, particularly as the number of interaction rounds increases (refer to Table 2). This improvement is primarily attributed to the fact that JCM refines suboptimal mask outputs from earlier rounds before they are referred in subsequent ones, thereby effectively mitigating the error accumulation inherent in the chain-like pipeline of multi-round segmentation.

We further construct a hybrid paradigm for comparison, which integrates an MLLM with a medical segmentation model. Specifically, we leverage the strong text–image reasoning capabilities of MLLMs [1, 3, 38] to interpret complex multi-round queries, and subsequently feed their generated reasoning outputs into a medical segmentation model to produce visual predictions. As shown in Tables 1 and 2, despite being supported by powerful MLLMs, these combined approaches still underperform compared with MediRound. We attribute this advantage to our model's end-to-end training on large-scale medical image–text pairs, which enables more coherent dynamic alignment between multimodal features than the two-stage combined paradigms. In addition, we include SegLLM [42]—the exploratory work on multi-round reasoning segmentation in natural images—in our comparison. The results indicate that while SegLLM performs well in natural images, it struggles when generalized to medical scenarios.

5.3. Vanilla Medical Referring Segmentation

To demonstrate MediRound's effectiveness in conventional single-round referring medical segmentation, we evaluate it against several prior related methods on the SA-Med2D-20M [48] benchmark. As summarized in Table 3, our model achieves strong performance, remaining highly competitive in traditional medical image segmentation. For context, we also report the segmentation results of IMIS-Net [6] and MedSAM [25] using conventional bounding box guidance.

Table 4. Ablation study on the choices of vision and MLLM backbones. Experiments are conducted on the MR-MedSeg val set.

Settings	Dice	gIoU	cIoU
Seg. Head Backbone			
SAM (ViT-H)	46.7	33.1	37.2
SAM-Med2D	53.9	45.3	55.5
MedSAM (LoRA)	54.6	44.9	54.4
MedSAM	55.8	46.5	55.8
MLLM Backbone			
LLaVA-v1.5 (LoRA)	53.4	42.1	53.3
LLaVA-Med (Frozen)	48.0	39.2	49.6
LLaVA-Med (LoRA)	55.8	46.5	55.8

5.4. Qualitative Analysis

We present qualitative comparisons in Figure 6. Existing methods largely fail in multi-round reasoning for medical segmentation, whereas MediRound can understand the current query and dialogue history for accurate segmentation.

5.5. Ablation Study

Choices of β in JCM. We investigate the impact of the threshold β in the Quality Judgement Module of JCM. As shown in Figure 7, the collaboration between JCM and MediRound achieves the best performance when $\boldsymbol{\beta = 0.6}$. This is likely because a smaller β causes many suboptimal results to lose the opportunity for refinement, while an excessively large β may instead disturb some high-quality predictions. *For the definition and role of β, see Algorithm 1.*

Choices of the Main Components. Table 4 summarizes the effects of different foundational MLLMs and segmentation head backbones. The results show that **LLaVA-Med** achieves superior performance owing to its strong multimodal alignment capability in medical contexts, while the **MedSAM** performs best as the segmentation head, benefiting from large-scale medical image pretraining.

6. Conclusion

This work introduces MEMR-Seg, a new task that advances medical image segmentation toward interactive, multi-round reasoning. By constructing the large-scale MR-MedSeg dataset and developing the MediRound baseline with a helpful Judgment & Correction Mechanism, this work demonstrates the feasibility and effectiveness of medical multi-round entity-level reasoning, providing insights for future research on interactive medical segmentation.

7. Appendix

Abstract Due to the space limit, we provide some implementation details and extra discussion in this Appendix. Specifically, the content of this document can be summarized as follows:

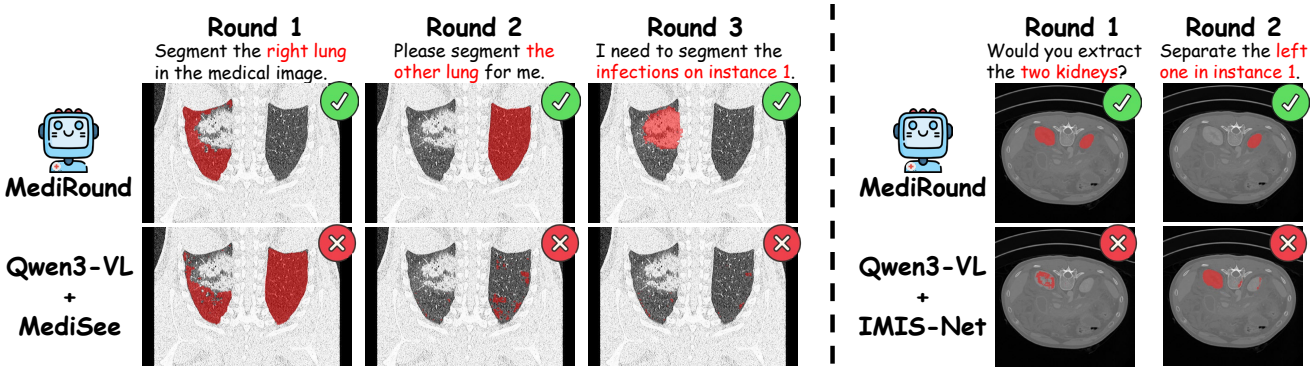

Figure 6. Qualitative comparison with different methods on medical multi-round interactive segmentation.

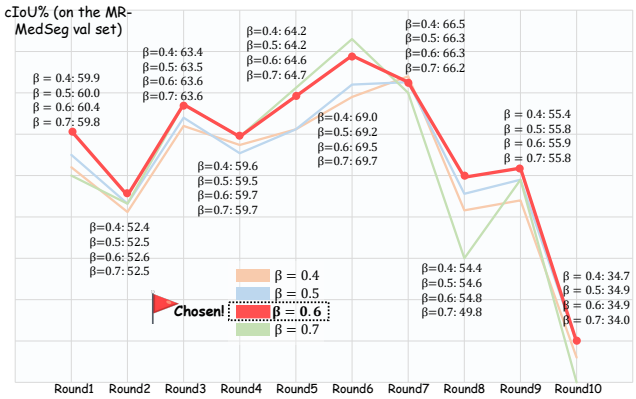

Figure 7. Ablation study on the threshold β value in JCM.

- We present the **training details of Judgment & Correction Mechanism (JCM)** in Appendix A.
- Additional training details of MediRound are provided in Appendix B.
- We conduct **ablation study on the effects of different strategies for extracting reference-mask information**, as detailed in Appendix C.
- We conduct **further analyses of the proposed MR-MedSeg** dataset in Appendix D.
- Additional visualization examples are provided in Appendix E to illustrate MediRound and MR-MedSeg. You can also watch the **MediRound demo video *(MediRound_Demo.mp4)*** for a more intuitive understanding.
- The limitations and future works of our paper are discussed in Appendix F.

A. Training the JCM

This section presents the training details of the Judgment & Correction Mechanism (JCM). The overall training pipeline of JCM is illustrated in Figure A.

A.1. Training Pipeline

The overall training pipeline of JCM is illustrated in Figure A. As shown in Figure A, LLaVA-Med takes x_{all} (denoting the full set of inputs) and produces the [SEG] token as

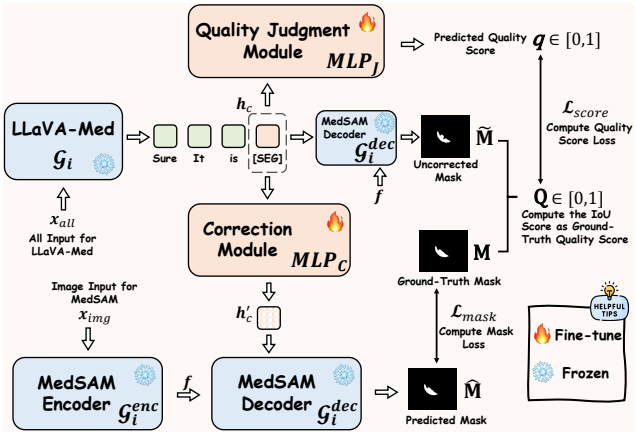

Figure A. Overview of the JCM training pipeline. *Please zoom in for improved clarity.*

output. The hidden feature of [SEG], h_c, is first fed into the Correction Module MLP_C, producing h_c'. The mask decoder $\mathcal{G}_i^{dec}$ then takes h_c' along with the visual features f (extracted by the vision backbone $\mathcal{G}_i^{enc}$) and outputs the predicted mask $\hat{\mathbf{M}}$. In parallel, $\mathcal{G}_i^{dec}$ takes h_c, f and outputs the uncorrected mask $\tilde{\mathbf{M}}$. The process can be formulated as:

$$h_c' = MLP_C(h_c), \quad \hat{\mathbf{M}} = \mathcal{G}_i^{dec}(f, h_c'), \quad \tilde{\mathbf{M}} = \mathcal{G}_i^{dec}(f, h_c). \tag{1}$$

Additionally, we also feed h_c into the Quality Judgment Module MLP_J, which outputs a quality score $q \in [0, 1]$ for h_c:

$$q = MLP_J(h_c), \quad q \in [0, 1] \tag{2}$$

We utilize the end-to-end trained MediRound weights to optimize the Correction Module MLP_C and the Quality Judgment Module MLP_J within the JCM. During the training of JCM, all parameters of the MediRound modules *(e.g., LLaVA-Med, MedSAM, etc.)* are frozen, and only the Correction Module MLP_C and the Quality Judgment Module MLP_J are trainable.

A.2. Optimization Strategy

For optimization, as illustrated in Figure A, the Correction Module MLP_C and the Quality Judgment Module MLP_J are jointly optimized using the mask loss $\mathcal{L}_{mask}$ and the quality score loss $\mathcal{L}_{score}$. For the quality score loss $\mathcal{L}_{score}$, we compute the Binary Cross-Entropy loss $\mathcal{L}_{bce}^{QJ}$ between the predicted quality score $q \in [0, 1]$ and the ground-truth quality score $\mathbf{Q} \in [0, 1]$. *The ground-truth quality score* $\mathbf{Q}$ *is obtained by computing the Intersection-over-Union (IoU) between the uncorrected mask* $\tilde{\mathbf{M}}$ *and the ground-truth mask* $\mathbf{M}$*, serving as a soft target in the Binary Cross-Entropy loss* $\mathcal{L}_{bce}^{QJ}$. The mask loss $\mathcal{L}_{mask}$ is also calculated between the predicted mask $\hat{\mathbf{M}}$ and the ground-truth mask $\mathbf{M}$, and it follows the same formulation as that used during MediRound training. The overall loss $\mathcal{L}_{JCM}$ can be formulated as:

$$\begin{aligned} \mathcal{L}_{JCM} &= \mathcal{L}_{bce}^{QJ} + \mathcal{L}_{mask}, \\ \mathcal{L}_{mask} &= \lambda_{bce}\mathcal{L}_{bce} + \lambda_{dice}\mathcal{L}_{dice}. \end{aligned} \tag{3}$$

B. MediRound Training Details

B.1. Training Parameter

In end-to-end training for MediRound, to preserve the fundamental capabilities of the LLM in $\mathcal{G}_i$ and save computing resources, we leverage LoRA to perform efficient fine-tuning on the LLM in $\mathcal{G}_i$, while completely freezing the vision backbone $\mathcal{G}_i^{enc}$ and LLaVA-Med vision encoder $\mathcal{G}_v^{enc}$. The mask decoder $\mathcal{G}_i^{dec}$ and the bounding box encoder $\mathcal{G}_b^{enc}$ are fully trainable.

B.2. Optimization Strategy

MediRound is trained through two supervisions. As for text generation, we compute the Auto-Regressive Cross-Entropy loss $\mathcal{L}_{txt}$ between the generated text output $\hat{y}_{txt}$ and the ground-truth text answer y_{txt}. For the generation of high-quality segmentation masks, the mask loss $\mathcal{L}_{mask}$ is calculated between the predicted mask $\hat{\mathbf{M}}$ and the ground-truth mask $\mathbf{M}$. And the mask loss $\mathcal{L}_{mask}$ is a weighted sum of the per-pixel Binary Cross-Entropy $\mathcal{L}_{bce}$ and the DICE loss $\mathcal{L}_{dice}$, with the weights determined by λ_{bce} and λ_{dice}. The overall loss $\mathcal{L}_{MediRound}$ is formulated as:

$$\begin{aligned} \mathcal{L}_{MediRound} &= \mathcal{L}_{txt} + \mathcal{L}_{mask}, \\ \mathcal{L}_{mask} &= \lambda_{bce}\mathcal{L}_{bce} + \lambda_{dice}\mathcal{L}_{dice}. \end{aligned} \tag{4}$$

C. Additional Ablation Study

We further investigate the impact of different strategies for extracting information from the reference mask. As shown in Table A, the experimental results indicate that using both the cropped image and the bounding box as reference-mask information yields the best performance.

Table A. Ablation study on the effects of different strategies for extracting reference-mask information. The experimental results are reported on the evaluation set of MR-MedSeg. $\mathcal{C}$: Cropped image input; $\mathcal{B}$: Bounding box input

$\mathcal{C}$	$\mathcal{B}$	Dice	gIoU	cIoU
✗	✗	41.9	32.5	38.4
✓	✗	55.4	45.8	56.0
✓	✓	55.8	46.5	55.8

D. Additional Analyses of MR-MedSeg

We provide additional analyses and clarifications of the proposed MR-MedSeg dataset to more clearly characterize its properties and data distribution.

D.1. How to Refer to Previous Results

In MR-MedSeg dataset, we primarily employ three phrasing strategies to refer to previous round results. The first is *"based on / ... / referring to the output of round* N*"*; the second is *"based on / ... / referring to instance* N*"*. The third is more specific: when referring directly to the immediately preceding round and when grammatical structure allows, we may simply use *"its ..."* to refer to the previous result.

D.2. Detailed Descriptions of Each Multi-Round Medical Segmentation Scenario

As illustrated in the Figure 2 (main text), we design five distinct types of interaction scenarios tailored for multi-round medical reasoning segmentation, each reflecting realistic use cases of interactive medical image segmentation:

- **Organ-Lesion:** In this scenario, the inter-instance relationships within the data are characterized by the associations between organs (or tissues) and the lesions located in those regions. These data first prompt the model to segment individual organs or tissues, and subsequently require it to segment the lesions that occur on these previously segmented structures. Consequently, accurate lesion segmentation requires the model to establish a cross-round understanding of the correspondence between lesions and the organs segmented in prior rounds.
- **Anatomical Structure Stratification:** In this scenario, the inter-instance relationships within the data correspond to the hierarchical anatomical relationships among different tissue structures. The model is first prompted to segment major anatomical regions, followed by the segmentation of substructures within these regions. Consequently, accurate segmentation of finer tissue structures necessitates cross-round understanding of the larger anatomical structures segmented in earlier rounds.
- **Organ/Tissue Attribute Relationship:** In this scenario, the inter-instance relationships within the data correspond

Table B. Data statistics of images, conversations, and maximum dialogue rounds across different multi-round interaction scenarios.

Scenario Type	Training Set			Validation Set			Test Set		
	# of Convs	# of Images	Max Rounds	# of Convs	# of Images	Max Rounds	# of Convs	# of Images	Max Rounds
Organ-Lesion	39711	27908	5	428	374	5	431	371	5
Anat. Struct. Strat.	45910	42913	12	235	235	12	233	233	12
Spatial Relationship	40969	13313	2	196	196	2	196	196	2
Strong Inferential Rel.	38139	22369	12	260	226	12	262	227	12
Org/Tissue Attr. Rel.	10205	8883	7	151	98	7	151	101	7

to the biological attribute associations among different organs or tissues. The data first prompts the model to segment a specific organ or tissue, and then, through the described attribute relationships, instructs it to segment the corresponding related structures. Consequently, accurate segmentation of medical entities in later rounds requires the model to reason over attribute relationships while maintaining cross-round understanding of previously segmented entities.

- **Spatial Relationship:** The inter-instance relationships in this scenario within the data correspond to the relative spatial relationships among different organs or tissues in a medical image. The data first prompts the model to segment a particular structure and subsequently, through the relative positional descriptions based on the previously segmented structures, requires it to segment other related structures. Consequently, accurate segmentation of medical entities in later rounds necessitates both the ability to reason over spatial relationships and cross-round understanding of previously segmented entities.
- **Strong Inferential Relationship:** Some medical images contain multiple medical entities of the same class. We transform such data to design a scenario characterized by *Strong Inferential Relationship*. Specifically, in the first round, we prompt the model to segment the initial entity through detailed referring expressions (e.g., *segment the left lung* or *segment the first left rib*). In subsequent rounds, we employ queries based on these *strong inferential relationships* to instruct the model to segment other instances of the same class (e.g., *segment the other lung* or *segment the next left rib*). For data of this scenario type, accurate segmentation of targets in subsequent rounds necessitates that the model maintain cross-round understanding of the entities segmented in earlier rounds, thereby requiring robust reasoning abilities across different segmentation rounds.

D.3. Category Distribution

As described in the main text, MR-MedSeg comprises 168 distinct categories of medical entities. The word cloud presented in Figure B (a) visually represents the distribution of classes within our dataset, highlighting the diverse range of medical entity categories upon which our dialogues are based. We also conduct a comprehensive analysis of the frequency distribution of each medical entity category across all dialogues, as illustrated in Figure B (b). The results indicate that the category occurrence frequencies in MR-MedSeg follow an approximately long-tailed distribution, which aligns well with real-world medical scenarios.

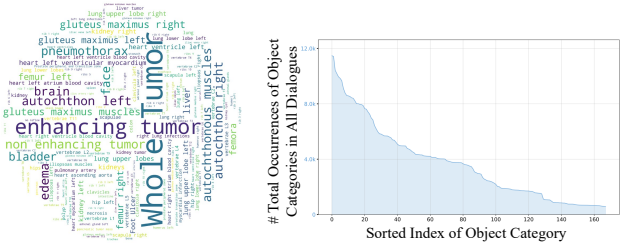

(a) (b)

Figure B. Analysis of the data structure in MR-MedSeg dataset. (a) Word cloud of MR-MedSeg; (b) Frequency distribution of each medical object across all the dialogues. *Please zoom in for improved clarity*.

D.4. Image Modality

As described in the main text, the proposed MR-MedSeg dataset encompasses a diverse set of imaging modalities. Specifically, it contains a total of 9 image modalities: *CT, Endoscopy, Dermoscopy, X-ray, MR-FLAIR, MR-T1C/MR-T1CE, MR-T1, MR-T2, and MR-ADC*. The diverse range of imaging modalities better simulates the complex variety of imaging types encountered in the real-world medical domain.

D.5. Data Statistics of Different Multi-Round Medical Segmentation Scenarios

To better characterize the data distribution across different scenarios, in Table B, we report the number of images and conversations for each multi-round interaction scenario, as well as the maximum dialogue rounds contained within each scenario.

E. More Visualization Examples

E.1. Additional Interactive Cases

We provide additional interactive cases of MediRound in Figure C. A demonstration video of our model, designated "*MediRound_Demo.mp4*", has also been included in the

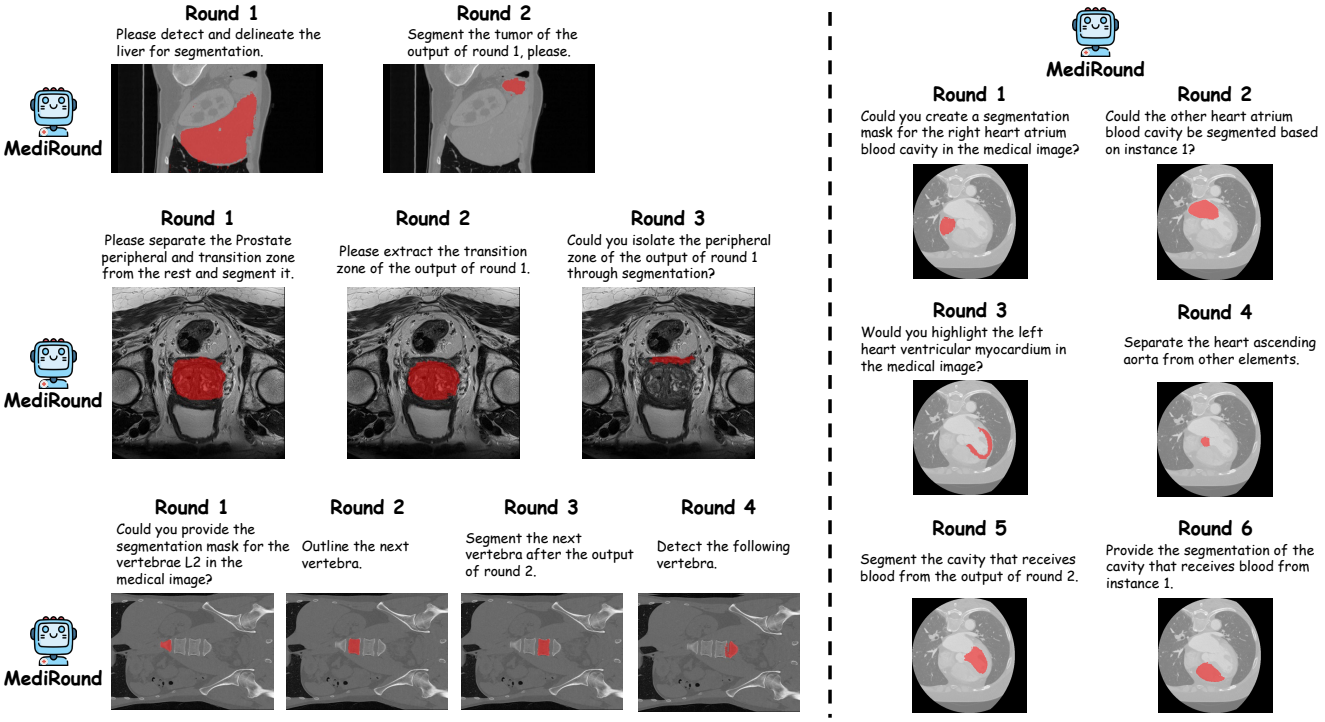

Figure C. Additional interactive cases of MediRound.

supplementary materials to provide a more detailed understanding.

F. Limitations and Future Works

In this section, we examine the limitations of the present work and outline potential directions for future research.

F.1. Multi-Object Segmentation in One Round

The current MediRound configuration restricts each round to segmenting a single medical entity, thereby preventing the model from handling multiple objects within the same interaction turn. This limitation may introduce inconvenience in certain practical clinical scenarios. Accordingly, in future work, we aim to extend MediRound to support multi-target segmentation within each dialogue round.

F.2. Processing Long Sequence

We observe that excessively long queries in each round can negatively affect the segmentation accuracy of MediRound. This reduced robustness to long sequences may be attributed to the inherent sequence-length limitations of transformer-based architectures.

F.3. Overfitting in the Segmentation Tasks

Trained on large-scale segmentation data, MediRound becomes specialized for segmentation tasks and nearly completely loses the core conversational capabilities of the MLLM. This reflects a common phenomenon of task-specific overfitting observed when MLLMs are adapted to downstream tasks. In future works, we aim to address this challenge by enabling the model to maintain a certain level of medical vision–language dialogue ability while still performing segmentation accurately.

F.4. More Modalities

Currently, MediRound is unable to process three-dimensional medical data or medical videos, which are frequently encountered in real-world clinical scenarios. In future work, we plan to extend MediRound to additional modalities, thereby overcoming its current restriction to two-dimensional images.

References

[1] Josh Achiam, Steven Adler, Sandhini Agarwal, Lama Ahmad, Ilge Akkaya, Florencia Leoni Aleman, Diogo Almeida, Janko Altenschmidt, Sam Altman, Shyamal Anadkat, et al. Gpt-4 technical report. *arXiv preprint arXiv:2303.08774*, 2023. 4, 6, 7, 8

[2] Michela Antonelli, Annika Reinke, Spyridon Bakas, Keyvan Farahani, Annette Kopp-Schneider, Bennett A Landman, Geert Litjens, Bjoern Menze, Olaf Ronneberger, Ronald M Summers, et al. The medical segmentation decathlon. *Nature communications*, 13(1):4128, 2022. 2

[3] Jinze Bai, Shuai Bai, Yunfei Chu, Zeyu Cui, Kai Dang, Xiaodong Deng, Yang Fan, Wenbin Ge, Yu Han, Fei Huang, et al. Qwen technical report. *arXiv preprint arXiv:2309.16609*, 2023. 6, 7, 8

[4] Ujjwal Baid, Satyam Ghodasara, Suyash Mohan, Michel Bilello, Evan Calabrese, Errol Colak, Keyvan Farahani, Jayashree Kalpathy-Cramer, Felipe C Kitamura, Sarthak Pati, et al. The rsna-asnr-miccai brats 2021 benchmark on brain tumor segmentation and radiogenomic classification. *arXiv preprint arXiv:2107.02314*, 2021. 2

[5] Junlong Cheng, Jin Ye, Zhongying Deng, Jianpin Chen, Tianbin Li, Haoyu Wang, Yanzhou Su, Ziyan Huang, Jilong Chen, Lei Jiang, et al. Sam-med2d. *arXiv preprint arXiv:2308.16184*, 2023. 7

[6] Junlong Cheng, Bin Fu, Jin Ye, Guoan Wang, Tianbin Li, Haoyu Wang, Ruoyu Li, He Yao, Junren Chen, JingWen Li, et al. Interactive medical image segmentation: A benchmark dataset and baseline. *arXiv preprint arXiv:2411.12814*, 2024. 2, 3, 6, 7, 8

[7] Michal Drozdzal, Eugene Vorontsov, Gabriel Chartrand, Samuel Kadoury, and Chris Pal. The importance of skip connections in biomedical image segmentation. In *International Workshop on Deep Learning in Medical Image Analysis*, pages 179–187. Springer, 2016. 3

[8] Yuxin Du, Fan Bai, Tiejun Huang, and Bo Zhao. Segvol: Universal and interactive volumetric medical image segmentation. *Advances in Neural Information Processing Systems*, 37:110746–110783, 2024. 3

[9] Nicholas Heller, Fabian Isensee, Dasha Trofimova, Resha Tejpaul, Zhongchen Zhao, Huai Chen, Lisheng Wang, Alex Golts, Daniel Khapun, Daniel Shats, et al. The kits21 challenge: Automatic segmentation of kidneys, renal tumors, and renal cysts in corticomedullary-phase ct. *arXiv preprint arXiv:2307.01984*, 2023. 2

[10] Murtadha D Hssayeni, Muayad S Croock, Aymen D Salman, Hassan Falah Al-Khafaji, Zakaria A Yahya, and Behnaz Ghoraani. Intracranial hemorrhage segmentation using a deep convolutional model. *Data*, 5(1):14, 2020. 2

[11] Xiaoshuang Huang, Hongxiang Li, Meng Cao, Long Chen, Chenyu You, and Dong An. Cross-modal conditioned reconstruction for language-guided medical image segmentation. *IEEE Transactions on Medical Imaging*, 2024. 2

[12] Xiaoshuang Huang, Lingdong Shen, Jia Liu, Fangxin Shang, Hongxiang Li, Haifeng Huang, and Yehui Yang. Towards a multimodal large language model with pixel-level insight for biomedicine. In *Proceedings of the AAAI Conference on Artificial Intelligence*, pages 3779–3787, 2025. 6, 7

[13] Yu Huang, Zelin Peng, Yichen Zhao, Piao Yang, Xiaokang Yang, and Wei Shen. Medseg-r: Reasoning segmentation in medical images with multimodal large language models. *arXiv preprint arXiv:2506.10465*, 2025. 2, 3

[14] Fabian Isensee, Paul F Jaeger, Simon AA Kohl, Jens Petersen, and Klaus H Maier-Hein. nnu-net: a self-configuring method for deep learning-based biomedical image segmentation. *Nature methods*, 18(2):203–211, 2021. 3

[15] David A Jaffray, Felicia Knaul, Michael Baumann, and Mary Gospodarowicz. Harnessing progress in radiotherapy for global cancer control. *Nature Cancer*, 4(9):1228–1238, 2023. 2

[16] Donggon Jang, Yucheol Cho, Suin Lee, Taehyeon Kim, and Dae-Shik Kim. Mmr: A large-scale benchmark dataset for multi-target and multi-granularity reasoning segmentation. *arXiv preprint arXiv:2503.13881*, 2025. 3, 5

[17] Alexander Kirillov, Eric Mintun, Nikhila Ravi, Hanzi Mao, Chloe Rolland, Laura Gustafson, Tete Xiao, Spencer Whitehead, Alexander C Berg, Wan-Yen Lo, et al. Segment anything. In *Proceedings of the IEEE/CVF international conference on computer vision*, pages 4015–4026, 2023. 3

[18] Xin Lai, Zhuotao Tian, Yukang Chen, Yanwei Li, Yuhui Yuan, Shu Liu, and Jiaya Jia. Lisa: Reasoning segmentation via large language model. In *Proceedings of the IEEE/CVF Conference on Computer Vision and Pattern Recognition*, pages 9579–9589, 2024. 2, 3

[19] Chunyuan Li, Cliff Wong, Sheng Zhang, Naoto Usuyama, Haotian Liu, Jianwei Yang, Tristan Naumann, Hoifung Poon, and Jianfeng Gao. Llava-med: Training a large language-and-vision assistant for biomedicine in one day. *Advances in Neural Information Processing Systems*, 36:28541–28564, 2023. 3, 5, 7

[20] Zihan Li, Yunxiang Li, Qingde Li, Puyang Wang, Dazhou Guo, Le Lu, Dakai Jin, You Zhang, and Qingqi Hong. Lvit: language meets vision transformer in medical image segmentation. *IEEE transactions on medical imaging*, 43(1): 96–107, 2023. 2

[21] Haotian Liu, Chunyuan Li, Qingyang Wu, and Yong Jae Lee. Visual instruction tuning. *Advances in neural information processing systems*, 36:34892–34916, 2023. 3, 5

[22] Shilong Liu, Zhaoyang Zeng, Tianhe Ren, Feng Li, Hao Zhang, Jie Yang, Qing Jiang, Chunyuan Li, Jianwei Yang, Hang Su, et al. Grounding dino: Marrying dino with grounded pre-training for open-set object detection. In *European Conference on Computer Vision*, pages 38–55. Springer, 2024. 7

[23] Ilya Loshchilov and Frank Hutter. Decoupled weight decay regularization. *arXiv preprint arXiv:1711.05101*, 2017. 7

[24] Timo Lüddecke and Alexander Ecker. Image segmentation using text and image prompts. In *Proceedings of the IEEE/CVF conference on computer vision and pattern recognition*, pages 7086–7096, 2022. 3

[25] Jun Ma, Yuting He, Feifei Li, Lin Han, Chenyu You, and Bo Wang. Segment anything in medical images. *Nature Communications*, 15(1):654, 2024. 3, 5, 7, 8

[26] Jun Ma, Yao Zhang, Song Gu, Cheng Ge, Shihao Mae, Adamo Young, Cheng Zhu, Xin Yang, Kangkang Meng, Ziyan Huang, et al. Unleashing the strengths of unlabelled data in deep learning-assisted pan-cancer abdominal organ quantification: the flare22 challenge. *The Lancet Digital Health*, 6(11):e815–e826, 2024. 2

[27] Victor Nauffal, Marcus DR Klarqvist, Matthew C Hill, Danielle F Pace, Paolo Di Achille, Seung Hoan Choi, Joel T Rämö, James P Pirruccello, Pulkit Singh, Shinwan Kany, et al. Noninvasive assessment of organ-specific and shared pathways in multi-organ fibrosis using t1 mapping. *Nature Medicine*, 30(6):1749–1760, 2024. 2

[28] Alireza Norouzi, Mohd Shafry Mohd Rahim, Ayman Altameem, Tanzila Saba, Abdolvahab Ehsani Rad, Amjad Rehman, and Mueen Uddin. Medical image segmentation methods, algorithms, and applications. *IETE Technical Review*, 31(3):199–213, 2014. 2

[29] Renjie Pi, Lewei Yao, Jiahui Gao, Jipeng Zhang, and Tong Zhang. Perceptiongpt: Effectively fusing visual perception into llm. In *Proceedings of the IEEE/CVF Conference on Computer Vision and Pattern Recognition*, pages 27124–27133, 2024. 3

[30] Rui Qian, Xin Yin, and Dejing Dou. Reasoning to attend: Try to understand how¡ seg¿ token works. *arXiv preprint arXiv:2412.17741*, 2024. 6, 7

[31] KKD Ramesh, G Kiran Kumar, K Swapna, Debabrata Datta, and S Suman Rajest. A review of medical image segmentation algorithms. *EAI Endorsed Transactions on Pervasive Health & Technology*, 7(27), 2021. 2

[32] Hanoona Rasheed, Muhammad Maaz, Sahal Shaji, Abdelrahman Shaker, Salman Khan, Hisham Cholakkal, Rao M Anwer, Eric Xing, Ming-Hsuan Yang, and Fahad S Khan. Glamm: Pixel grounding large multimodal model. In *Proceedings of the IEEE/CVF Conference on Computer Vision and Pattern Recognition*, pages 13009–13018, 2024. 3

[33] Jeff Rasley, Samyam Rajbhandari, Olatunji Ruwase, and Yuxiong He. Deepspeed: System optimizations enable training deep learning models with over 100 billion parameters. In *Proceedings of the 26th ACM SIGKDD international conference on knowledge discovery & data mining*, pages 3505–3506, 2020. 7

[34] Olaf Ronneberger, Philipp Fischer, and Thomas Brox. U-net: Convolutional networks for biomedical image segmentation. In *Medical image computing and computer-assisted intervention–MICCAI 2015: 18th international conference, Munich, Germany, October 5-9, 2015, proceedings, part III 18*, pages 234–241. Springer, 2015. 2, 3

[35] Rina D Rudyanto, Sjoerd Kerkstra, Eva M Van Rikxoort, Catalin Fetita, Pierre-Yves Brillet, Christophe Lefevre, Wenzhe Xue, Xiangjun Zhu, Jianming Liang, Ilkay Öksüz, et al. Comparing algorithms for automated vessel segmentation in computed tomography scans of the lung: the vessel12 study. *Medical image analysis*, 18(7):1217–1232, 2014. 2

[36] Anindo Saha, Matin Hosseinzadeh, and Henkjan Huisman. End-to-end prostate cancer detection in bpmri via 3d cnns: effects of attention mechanisms, clinical priori and decoupled false positive reduction. *Medical image analysis*, 73: 102155, 2021.

[37] Arnaud Arindra Adiyoso Setio, Alberto Traverso, Thomas De Bel, Moira SN Berens, Cas Van Den Bogaard, Piergiorgio Cerello, Hao Chen, Qi Dou, Maria Evelina Fantacci, Bram Geurts, et al. Validation, comparison, and combination of algorithms for automatic detection of pulmonary nodules in computed tomography images: the luna16 challenge. *Medical image analysis*, 42:1–13, 2017. 2

[38] Gemini Team, Rohan Anil, Sebastian Borgeaud, Jean-Baptiste Alayrac, Jiahui Yu, Radu Soricut, Johan Schalkwyk, Andrew M Dai, Anja Hauth, Katie Millican, et al. Gemini: a family of highly capable multimodal models. *arXiv preprint arXiv:2312.11805*, 2023. 6, 7, 8

[39] Qinyue Tong, Ziqian Lu, Jun Liu, Yangming Zheng, and Zheming Lu. Medisee: Reasoning-based pixel-level perception in medical images. *arXiv preprint arXiv:2504.11008*, 2025. 2, 3, 6, 7

[40] Junchi Wang and Lei Ke. Llm-seg: Bridging image segmentation and large language model reasoning. In *Proceedings of the IEEE/CVF Conference on Computer Vision and Pattern Recognition*, pages 1765–1774, 2024. 2

[41] Risheng Wang, Tao Lei, Ruixia Cui, Bingtao Zhang, Hongying Meng, and Asoke K Nandi. Medical image segmentation using deep learning: A survey. *IET image processing*, 16(5): 1243–1267, 2022. 2

[42] XuDong Wang, Shaolun Zhang, Shufan Li, Konstantinos Kallidromitis, Kehan Li, Yusuke Kato, Kazuki Kozuka, and Trevor Darrell. Segllm: Multi-round reasoning segmentation. *arXiv preprint arXiv:2410.18923*, 2024. 2, 3, 5, 6, 7, 8

[43] Yueyue Wang, Liang Zhao, Manning Wang, and Zhijian Song. Organ at risk segmentation in head and neck ct images using a two-stage segmentation framework based on 3d u-net. *IEEE Access*, 7:144591–144602, 2019. 2

[44] Ronald J Williams and David Zipser. A learning algorithm for continually running fully recurrent neural networks. *Neural computation*, 1(2):270–280, 1989. 6, 7

[45] Ke Yan, Xiaosong Wang, Le Lu, and Ronald M Summers. Deeplesion: automated mining of large-scale lesion annotations and universal lesion detection with deep learning. *Journal of medical imaging*, 5(3):036501–036501, 2018. 2

[46] Zhonghao Yan, Muxi Diao, Yuxuan Yang, Jiayuan Xu, Kaizhou Zhang, Ruoyan Jing, Lele Yang, Yanxi Liu, Kongming Liang, and Zhanyu Ma. Medreasoner: Reinforcement learning drives reasoning grounding from clinical thought to pixel-level precision. *arXiv preprint arXiv:2508.08177*, 2025. 2, 3

[47] Senqiao Yang, Tianyuan Qu, Xin Lai, Zhuotao Tian, Bohao Peng, Shu Liu, and Jiaya Jia. Lisa++: An improved baseline for reasoning segmentation with large language model. *arXiv preprint arXiv:2312.17240*, 2023. 2, 5

[48] Jin Ye, Junlong Cheng, Jianpin Chen, Zhongying Deng, Tianbin Li, Haoyu Wang, Yanzhou Su, Ziyan Huang, Jilong Chen, Lei Jiang, et al. Sa-med2d-20m dataset: Segment anything in 2d medical imaging with 20 million masks. *arXiv preprint arXiv:2311.11969*, 2023. 2, 3, 4, 8

[49] Ao Zhang, Yuan Yao, Wei Ji, Zhiyuan Liu, and Tat-Seng Chua. Next-chat: An lmm for chat, detection and segmentation. *arXiv preprint arXiv:2311.04498*, 2023. 3, 5

[50] Theodore Zhao, Yu Gu, Jianwei Yang, Naoto Usuyama, Ho Hin Lee, Sid Kiblawi, Tristan Naumann, Jianfeng Gao, Angela Crabtree, Jacob Abel, et al. A foundation model for joint segmentation, detection and recognition of biomedical objects across nine modalities. *Nature methods*, pages 1–11, 2024. 2, 3, 6, 7

[51] Zongwei Zhou, Md Mahfuzur Rahman Siddiquee, Nima Tajbakhsh, and Jianming Liang. Unet++: A nested u-net architecture for medical image segmentation. In *Deep learning in medical image analysis and multimodal learning for clinical decision support: 4th international workshop, DLMIA 2018, and 8th international workshop, ML-CDS 2018, held in conjunction with MICCAI 2018, Granada, Spain, September 20, 2018, proceedings 4*, pages 3–11. Springer, 2018. 3